




Cite this: *RSC Adv.*, 2017, 7, 29143

Selective hydrogenation of *p*-chloronitrobenzene over an Fe promoted Pt/AC catalyst

Hu Chen, Daiping He, * Qingqing He, Ping Jiang,  Gongbing Zhou and Wensheng Fu

Activated carbon supported Pt (Pt/AC) and Fe modified Pt (Pt-Fe/AC) catalysts have been investigated for selective hydrogenation of *p*-chloronitrobenzene to *p*-chloroaniline. It was found that the incorporation of an appropriate amount of Fe (4 wt%) resulted in a remarkable increase in activity and selectivity to *p*-chloroaniline, and the catalytic hydrodechlorination over the catalyst was fully suppressed at complete conversion of *p*-chloronitrobenzene. X-ray photoelectron spectroscopy (XPS) revealed the electron transfer from Pt nanoparticles to Fe₂O₃, leading to the electron-deficient state of the Pt nanoparticles in the present catalyst, which is responsible for improved performance of the Pt-Fe/AC catalyst for *p*-chloronitrobenzene hydrogenation to *p*-chloroaniline.

Received 26th April 2017

Accepted 28th May 2017

DOI: 10.1039/c7ra04700b

rsc.li/rsc-advances

1 Introduction

The reduction of chloronitrobenzenes to chloroanilines is significant in organic synthesis because the chloroanilines are the key intermediates of pharmaceuticals, polymers, pesticides, explosives, fibers, dyes and cosmetics.¹ The traditional methods that use either the Fe/HCl system (Bechamp reaction) or metal sulfides inevitably generate large amounts of waste, which requires costly and laborious separation and disposal.² Synthesis of chloroanilines using catalytic hydrogenation starting with chloronitrobenzenes offers several advantages over chemical reduction, including cheap hydrogen, easy product separation and a nonpolluting process. A severe problem related to the catalytic hydrogenation has been the co-occurrence of the catalytic hydrodechlorination reaction of the substrates,^{3–5} which significantly limits the selectivity to chloroanilines and leads to a lot of wastes. Furthermore, hydrogen chloride produced from the hydrodechlorination is also corrosive to the reactor. It is highly desirable to develop heterogeneous catalysts that would ensure the selective reduction of the nitro groups while leave intact of the carbon–chlorine bond in the same molecule. Many efforts have been devoted to performing selective hydrogenation of chloronitrobenzenes to corresponding chloroanilines over a plentiful of metal catalysts,^{6–11} including Pt, Pd, Au, Ru, Ni and Ag. The gold catalyst offers the highest selectivity of chloroanilines for this hydrogenation,^{12,13} but platinum seems to be the best catalyst for minimizing dechlorination combined with a fast rate of reduction of the nitro group and being highly resistant to

deactivation.¹⁴ In most cases, high selectivity is always achieved at the expense of activity by introducing either transition-metal salts or additives that partly poison the active sites.^{15–17} The choice of components is critical in developing an efficient and viable catalyst, and due attention should be paid to the interaction between active metal and promoter, since the nature of this interaction plays an important role in shaping the activity, selectivity and stability of the catalyst. Mahata *N et al.*¹⁸ studied the influence of Cu on the catalytic properties of Pt/C for the hydrogenation of chloronitrobenzenes. It is found that the strong interactions between Pt and Cu result in partial coverage of the Pt surface by Cu. The superficial Cu species activate the N=O bond of chloronitrobenzene and also inhibit the adsorption of the desired product chloroaniline. Thus, the bimetallic catalysts exhibited excellent performance in producing selectively chloroanilines (>99%) in comparison to the Pt/AC catalyst. Moreover, the high catalytic activity of the Pt nanoclusters was maintained.

In this paper, we report the promotional effect of Fe on the catalytic performance of Pt/C catalyst. The possible function of Fe in Pt-Fe/AC catalysts is discussed on the basis of catalyst characterization and catalytic results.

2 Experimental

2.1 Catalyst preparation

An activated carbon (AC) sample was obtained from Chongqing Chuandong Chemical Company and was crushed into 220–250 mesh powder. It was washed with distilled water, then dried at 383 K overnight and calcined in flowing air at 523 K for 3 h. The Pt-Fe/AC catalyst was prepared by a wet impregnation technique. Typically, 2.0 g of activated carbon with BET surface area of 411 m² g^{−1} was added to 50 mL aqueous Fe(NO₃)₃ (0.03 mol

Key Lab of Green Synthesis and Applications, College of Chemistry, Chongqing Normal University, Chongqing 401331, China. E-mail: hedaiping@126.com; Fax: +86-23-6536-2777; Tel: +86-23-6591-0309



L^{-1}) and the suspension was stirred for 24 h. Then, 1.58 mL aqueous H_2PtCl_6 ($3.8 \times 10^{-3} \text{ mol L}^{-1}$) was added dropwise to the mixture for 24 h upon continuous stirring. The deposition of Pt and Fe nanoparticles from the aqueous solution occurred when a stoichiometric excess of aqueous NaBH_4 (0.5 mol L^{-1}) was added dropwise to the mixture. Stirring was continued for a further 5 h. The solids were filtered and washed thoroughly with distilled water until free of chloride ions. The obtained sample was dried at 383 K for 10 h and calcined in flowing air at different temperature for 5 h. The platinum, iron in the catalyst was 0.29 wt% and 3.86 wt% according to ICP-AES analysis, respectively.

2.2 Catalyst characterization

The platinum and iron contents in the 0.3% Pt–4% Fe/AC catalyst were analyzed by means of inductively coupled plasma-atomic emission spectroscopy (ICP-AES) after the sample was dissolved in aqua regia. X-ray powder diffraction (XRD) patterns were recorded on a Rigaku D/Max Ultima IV X-ray diffractometer using Cu $\text{K}\alpha$ radiation with accelerating voltage of 40 kV and current of 30 mA. Transmission electron microscopy (TEM) measurement was performed on a JEOL JEM-2000EX microscope operated at an accelerating voltage of 120 kV. An energy-dispersive X-ray (EDX) spectroscopic detecting unit was used to collect the EDX spectra for elemental analysis. X-ray photoelectron spectra (XPS) were obtained on an ESCALAB 250 X-ray photoelectron spectroscopy using Mg- $\text{K}\alpha$ X-ray as the excitation source. XPS spectra were calibrated based on the graphite C 1s peak at 284.6 eV.

2.3 Catalyst testing

The catalytic hydrogenation was carried out with magnetic stirring (900 rpm) in a 60 mL Teflon-lined stainless steel autoclave containing 1.0 g of *p*-chloronitrobenzene (*p*-CNB) in 8.0 mL ethanol (solvent). The catalyst used in each run of the reaction was 20.0 mg. The reactor was flushed one time with 0.5 MPa N_2 and then four times with 0.5 MPa H_2 before it was pressurized to the desired H_2 pressure and placed in a heat installation maintained at the reaction temperature. The reaction was stopped at a selected time by cooling the reactor in a ice water bath. The products were analyzed by GC (GC9890) with an SE-30 capillary column and an FID as detector, using *o*-xylene as an internal standard.

3 Results and discussion

3.1 Catalyst characterization

The XRD patterns of the AC support and 0.3% Pt–4% Fe/AC catalyst are shown in Fig. 1. The AC support shows the characteristic diffraction peaks of graphitized activated carbon at $2\theta = 24.3^\circ$, 35.4° and 43.2° .¹⁹ The minor peaks at 20.7° , 26.5° , 39.4° , 50.1° and 68.1° are attributed to the presence of trace quantity of silica.²⁰ The XRD pattern of the 0.3% Pt–4% Fe/AC catalyst is similar to that of the AC support as we can see from Fig. 1b. No characteristic diffraction peaks at 39.9° , 46.4° , 67.5° index to (111), (200), (220) planes of metallic Pt²¹ and 44.4°

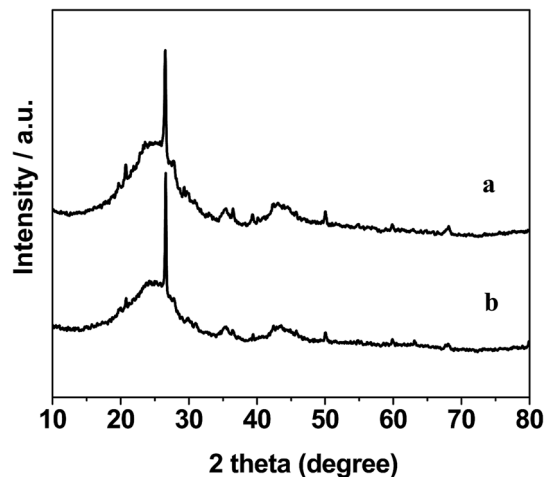


Fig. 1 XRD patterns of AC (a) and 0.3% Pt–4% Fe/AC (b).

assigned to Fe (110) plane²² were detected in the 0.3% Pt–4% Fe/AC catalyst, probably because of the low percentage of metals on the catalyst and/or the small particle size.

Fig. 2 shows the representative TEM images of the 0.3% Pt–4% Fe/AC catalyst. As can be seen from the TEM image (Fig. 2a), small black spots can be discerned from the background over the 0.3% Pt–4% Fe/AC catalyst. A combined EDX analysis showed that the signal of Pt and Fe could be detected in the small black spots (Fig. 2b). Therefore, we conclude that the small black spots in Fig. 2a are the images of the Pt and Fe species. The Fe and Pt particles in the 0.3% Pt–4% Fe/AC

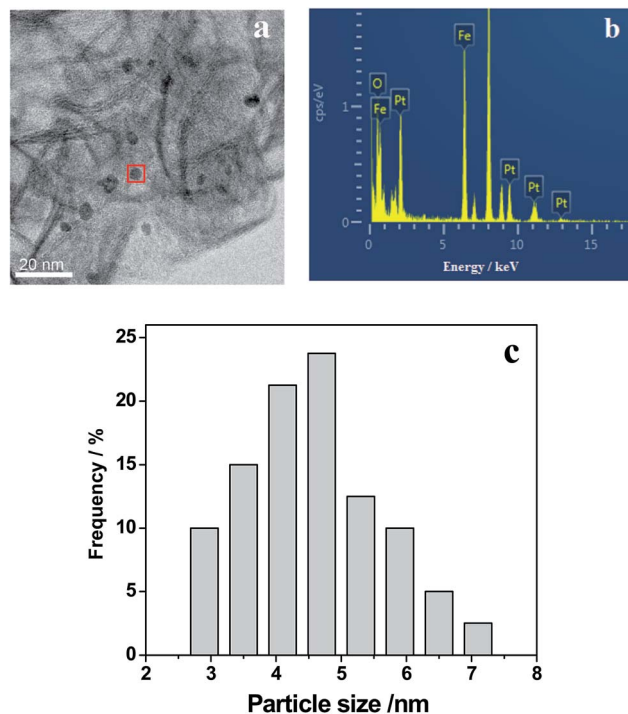


Fig. 2 TEM image of 0.3% Pt–4% Fe/AC (a), EDX spectra of the selected area (b) and size distributions of Pt–Fe particles in the catalyst (c).



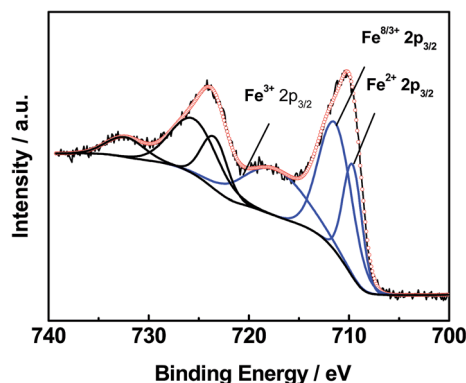


Fig. 3 XPS spectrum of Fe $2p_{3/2}$ for 0.3% Pt–4% Fe/AC.

catalyst have an average diameter of 4.5 nm, with a size distribution from 3 to 7 nm (Fig. 2c), which is consistent with the absence of characteristic diffraction peaks of Fe and Pt in the XRD pattern of the 0.3% Pt–4% Fe/AC, suggesting that the Fe and Pt species on AC support are in a homogenous dispersion without any obvious aggregation.

XPS analyses of the 0.3% Pt/AC and 0.3% Pt–4% Fe/AC catalysts were performed. The Fe 2p spectrum of the 0.3% Pt–4% Fe/AC can be deconvoluted three peaks (Fig. 3). The peaks can be assigned to Fe^{3+} in Fe_2O_3 , $\text{Fe}^{8/3+}$ in Fe_3O_4 and Fe^{2+} in FeO, respectively.²³ It is evident that the calcination of the 0.3% Pt–4% Fe/AC at 473 K in air leads to the formation of Fe_2O_3 on AC. Fig. 4 presents the Pt 4f spectra of the 0.3% Pt/AC and 0.3% Pt–4% Fe/AC catalysts. The Pt $4f_{7/2}$ photoelectron peak of the 0.3% Pt/AC catalyst is observed at 71.2 eV (Fig. 4a), which is consistent with the characteristic peak of Pt $4f_{7/2}$ for metallic Pt at 71.1 eV.²⁴ However, the binding energy of the Pt $4f_{7/2}$ level in the 0.3% Pt–4% Fe/AC catalyst (Fig. 4b) is 0.9 eV higher than that of metallic Pt. This reveals the electron transfer and the electron-deficient state of the Pt nanoparticles in the 0.3% Pt–4% Fe/AC catalyst. Wang *et al.*²⁵ also observed the same phenomenon in the Pt/ γ - Fe_2O_3 catalyst. Based on these results, we believe that the electron transfer may occur from the Pt particles to the Fe_2O_3 in the 0.3% Pt–4% Fe/AC catalyst.

3.2 Catalytic performance

Table 1 shows the catalytic properties of the 4% Fe/AC, 0.3% Pt/AC and 0.3% Pt–Fe/AC catalysts for hydrogenation of *p*-CNB at 303 K, 1.0 MPa H_2 . No reaction of *p*-CNB was observed in the absence of the catalyst and over the 4% Fe/AC catalyst. The conversion of *p*-CNB over the 0.3% Pt/AC catalyst was 37% for 40 minutes. When the same 0.3% Pt/AC was loaded with 4% Fe, however, a dramatically high *p*-CNB conversion (65%) was achieved under the same reaction conditions, and the selectivity to the desired product *p*-CAN also increased from 84.0% to 94.2%, which may be attributed to Fe_xO_y species activated the N=O bond which becomes highly susceptible to hydrogen attack.²⁶ When Fe loading amount further increases from 4 wt% to 6 wt%, the conversion of *p*-CNB decreases from 65% to 33%, which may be caused by partial coverage of the Pt surface by excess Fe_xO_y . Interestingly, the undesired hydrodechlorination

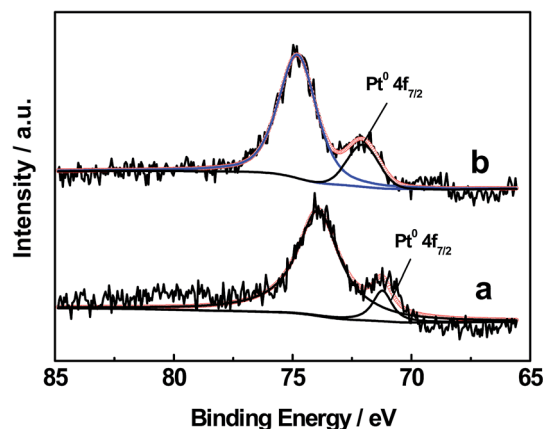


Fig. 4 XPS spectra of Pt $4f_{5/2}$ for 0.3% Pt/AC (a) and 0.3% Pt–4% Fe/AC (b).

reaction observed over the Pt/AC was not detected over the 0.3% Pt–4% Fe/AC catalyst. Special attention was paid to distinguish byproducts of the *p*-CNB hydrogenation reactions with GC-MS. Any byproduct that amounted to 0.1% in the reaction mixture can be unambiguously detected in our method of product analysis. We did not detect any by-products derived from the hydrodechlorination over the 0.3% Pt–4% Fe/AC catalyst, even when the reaction time was extended by 30 minutes after *p*-CNB was exhausted, which indicates that the undesired hydrodechlorination reaction usually observed over other metal catalysts^{27–29} can be successfully avoided over the catalyst. XPS data indicate that the electron transfer occurred from Pt to Fe_2O_3 make the Pt nanoparticles in the 0.3% Pt–4% Fe/AC catalyst an electron-deficient state. The electron-deficient state of the Pt particles could weaken the extent of electron feedback from the Pt particles to the aromatic ring in chloroanilines and suppressed the hydrodechlorination reaction.²⁵ Therefore, the high selectivity of *p*-CAN over the 0.3% Pt–4% Fe/AC catalyst may attribute to the electron-deficient state of the Pt nanoparticles.

Table 1 Catalytic results of selective hydrogenation of *p*-CNB over different catalysts^a

Catalyst	<i>p</i> -CNB conv./% (min)	Sel. (%)		
		<i>p</i> -CAN	AN ^b	Others ^c
4% Fe/AC	n.d. (40)	n.d.	n.d.	n.d.
0.3% Pt/AC	37 (40)	84.0	n.d.	16.0
0.3% Pt–2% Fe/AC	50 (40)	92.6	n.d.	7.4
0.3% Pt–4% Fe/AC	65 (40)	94.2	n.d.	5.8
0.3% Pt–4% Fe/AC	100 (90)	100	n.d.	n.d.
0.3% Pt–4% Fe/AC	100 (120)	100	n.d.	n.d.
0.3% Pt–6% Fe/AC	33 (40)	92.7	n.d.	7.3

^a n.d.: not detected. ^b AN refers to aniline. ^c Other products were *p*-chloronitrosobenzene, 4,4'-dichloroazoxybenzene and 4,4'-dichloroazobenzene. Reaction conditions: 20.0 mg catalyst, 1.0 g *p*-CNB in 8.0 mL ethanol (solvent), 303 K, 1.0 MPa H_2 .



Table 2 Effect of calcination temperature on catalytic performance of 0.3% Pt–4% Fe/AC for *p*-CNB hydrogenation

Calci. temp./K	<i>p</i> -CNB conv./%	Sel./%		
		<i>p</i> -CAN	AN ^a	Others ^a
383	33	91.4	n.d.	8.6
473	65	94.2	n.d.	5.8
573	57	93.8	n.d.	6.2
623	51	93.2	n.d.	6.8

^a See the note in Table 1. Reaction conditions are the same as in Table 1.**Table 3** Effect of reaction temperature on catalytic performance of 0.3% Pt–4% Fe/AC for *p*-CNB hydrogenation

React. temp./K	<i>p</i> -CNB conv./%	Sel./%		
		<i>p</i> -CAN	AN ^a	Others ^a
303	65	94.2	n.d.	5.8
313	92	96.3	n.d.	3.7
323	100	98.9	n.d.	1.1
333	100	100	n.d.	n.d.

^a See the note in Table 1. Other reaction conditions are the same as in Table 1.

3.3 Effect of calcination temperature

The hydrogenation properties of the 0.3% Pt–4% Fe/AC calcined at different temperature are also investigated, and the results are listed in Table 2. From Table 2, we can see that different calcination temperature of the 0.3% Pt–4% Fe/AC has significant influence on the hydrogenation of *p*-CNB. The 0.3% Pt–4% Fe/AC calcined at 473 K shows the best catalytic activity and selectivity towards *p*-CAN, which could be the result of the favorable formation of Fe₂O₃ on AC at 473 K, and the sintering of the Pt nanoparticles at higher calcination temperature (>473 K).

3.4 Effect of reaction conditions

The reaction temperature also plays a significant role in the *p*-CNB hydrogenation reaction (Table 3). The conversion of *p*-CNB and selectivity to *p*-CAN was 65% and 94.2% at 303 K,

Table 4 Effect of H₂ pressure on catalytic performance of 0.3% Pt–4% Fe/AC for *p*-CNB hydrogenation

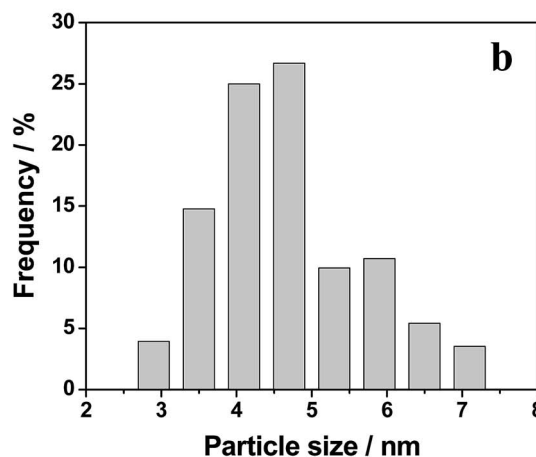
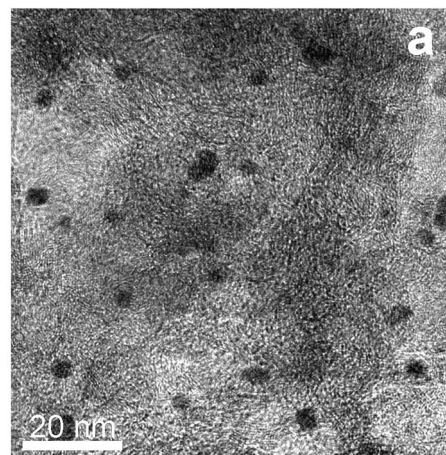
H ₂ pressure/MPa	<i>p</i> -CNB conv./%	Sel./%		
		<i>p</i> -CAN	AN ^a	Others ^a
0.5	30	92.9	n.d.	7.1
1.0	65	94.2	n.d.	5.8
2.0	100	98.5	n.d.	1.5
3.0	100	100	n.d.	n.d.

^a See the note in Table 1. Other reaction conditions are the same as in Table 1.**Table 5** Reusability of 0.3% Pt–4% Fe/AC catalyst for selective hydrogenation of *p*-CNB

Cycle number	<i>p</i> -CNB conv. (%)	Sel. (%)		
		<i>p</i> -CAN	AN ^a	Others ^a
1	65	94.2	n.d.	5.8
2	52	92.7	n.d.	7.3
3	42	92.5	n.d.	7.5
4	42	92.3	n.d.	7.7

^a See the note in Table 1. Reaction conditions are the same as in Table 1.

respectively. The conversion increased significantly to 100% and the selectivity reached 100% without formation of any dechlorination product when the reaction temperature increased from 303 K to 333 K. The byproducts produced in the reaction can be further hydrogenated to the desired product *p*-CAN. These data demonstrate that the undesired further hydrogenation of *p*-CAN can be avoided over the 0.3% Pt–4% Fe/AC catalyst in a broad window (303–333 K).

**Fig. 5** TEM image of the 0.3% Pt–4% Fe/AC after catalysis (a) and size distributions of Pt–Fe particles in the catalyst (b).

This advantage of the catalyst is clearly shown by the catalytic properties under the elevated H_2 pressure (Table 4). The conversion of *p*-CNB and selectivity to *p*-CAN was 30% and 92.9% at 0.5 MPa H_2 , respectively. The conversion increased to 100% and the selectivity reached 98.5% at 2.0 MPa H_2 . It is interesting to note that any by-products derived from the hydrodechlorination were not detected, even when all of the *p*-CNB was exhausted under 3.0 MPa, which demonstrates a remarkable feature of the 0.3% Pt–4% Fe/AC catalyst for avoiding successfully any occurrence of the further hydrogenation of *p*-CAN even when very high H_2 pressure is used for the reaction.

3.5 Catalyst stability

The recycling procedure of the 0.3% Pt–4% Fe/AC catalyst was performed for examining the stability of the catalyst. The catalyst after reaction was separated by centrifugation, washed with ethanol, dried under vacuum and then reused for the same reaction. As shown in Table 5, both conversion and selectivity did not exhibit a considerable decrease for at least 4 cycles. We checked the Pt, Fe content in the recovered catalyst after 4 cycles and found that there was only a slight loss of Pt (0.02 wt%) and Fe (0.35 wt%) in the recovered catalyst. TEM analysis showed good dispersion of Pt–Fe particles in the recovered 0.3% Pt–4% Fe/AC (Fig. 5a). The average Pt–Fe particle size was 4.6 nm, with a size distribution from 3 to 7 nm (Fig. 5b), which is similar to that in the as-prepared fresh 0.3% Pt–4% Fe/AC catalyst (4.5 nm) (Fig. 2c). The as-prepared 0.3% Pt–4% Fe/AC catalyst showed high stability.

4 Conclusion

In this study, we have prepared Fe modified Pt nanoparticles over activated carbon and investigated their catalytic performance on the chemoselective hydrogenation of *p*-chloronitrobenzene. It was found that the incorporation of an appropriate amount of Fe (4 wt%) resulted in a remarkable increase in activity, and the selectivity to *p*-chloronitrobenzene could be up to 100% at complete conversion of *p*-chloronitrobenzene over 0.3% Pt–4% Fe/AC catalyst even at high temperature and H_2 pressure. X-ray photoelectron spectroscopy revealed the formation of Fe_2O_3 and the electron transfer from Pt nanoparticles to Fe_2O_3 , leading to the electron-deficient state of the Pt nanoparticles in the present catalyst, which are responsible for the improved performance of 0.3% Pt–4% Fe/AC catalyst for *p*-chloronitrobenzene hydrogenation to *p*-chloroaniline. High reaction temperature and H_2 pressure are favorable for *p*-CNB hydrogenation to *p*-CAN over the 0.3% Pt–4% Fe/AC catalyst.

Acknowledgements

This work was supported by the Science and Technology Innovation Project of Chongqing (cstc2016shmszx20004) and Project of International Science and Technology Cooperation in Chongqing (cstc2014gjhz20002).

References

- 1 R. S. Downing, P. J. Kunkeler and H. van Bekkum, *Catal. Today*, 1997, **37**, 121.
- 2 H. U. Blaser, U. Siegrist, H. Steiner and M. Studer, in *Fine Chemicals through Heterogeneous Catalysis*, Wiley-VCH, Weinheim, 2001, pp. 389–406.
- 3 M. H. Liu, X. X. Mo, Y. Y. Liu, H. L. Xiao, Y. Zhang, J. Y. Jing, V. Colvin and W. W. Yu, *Appl. Catal., A*, 2012, **439–440**, 192.
- 4 S. Ichikawa, T. Seki and T. Ikariya, *Adv. Synth. Catal.*, 2014, **356**, 2643.
- 5 A. B. Dongil, L. Pastor-Pérez, J. L. G. Fierro, N. Escalona and A. Sepúlveda-Escriban, *Catal. Commun.*, 2016, **75**, 55.
- 6 F. Cárdenas-Lizana, S. Gómez-Quero and M. A. Keane, *Appl. Catal., A*, 2008, **334**, 199.
- 7 L. N. Liu, L. N. Xing, C. X. Cheng, L. X. Xia and H. Y. Liu, *RSC Adv.*, 2016, **6**, 31871.
- 8 Y. C. Liu, C. Y. Huang and Y. W. Chen, *Ind. Eng. Chem. Res.*, 2006, **45**, 62.
- 9 Y. Y. Fan, H. L. Xiao, N. Sui, M. H. Liu and W. W. Yu, *RSC Adv.*, 2014, **4**, 11788.
- 10 E. Bertolucci, R. Bacsá, A. Benyounes, A. M. Raspolli-Gallett, M. R. Axet and P. Serp, *ChemCatChem*, 2015, **7**, 2971.
- 11 F. Cardenas-Lizana, D. Lamey, N. Perret, S. Gomez-Quero, L. Kiwi-Minsker and M. A. Keane, *Catal. Commun.*, 2015, **21**, 46.
- 12 C. H. Camposa, M. Jofréa, C. C. Torresa, B. Pawelech, J. L. G. Fierrob and P. Reyesa, *Appl. Catal., A*, 2014, **482**, 127.
- 13 D. P. He, X. D. Jiao, P. Jiang, J. Wang and B. Q. Xu, *Green Chem.*, 2012, **14**, 111.
- 14 M. H. Liu, W. Y. Yu and H. F. Liu, *J. Mol. Catal. A: Chem.*, 1999, **138**, 295.
- 15 M. Makosch, W. I. Lin, V. Bumbálek, J. Sá, J. W. Medlin, K. Hungerbühler and J. A. van Bokhoven, *ACS Catal.*, 2012, **2**, 2079.
- 16 S. Furukawa, Y. Yoshida and T. Komatsu, *ACS Catal.*, 2014, **4**, 1441.
- 17 K. Möbus, D. Wolf, H. Benischke, U. Dittmeier, K. Simon, U. Packruhn, R. Jantke, S. Weidlich, C. Weber and B. S. Chen, *Top. Catal.*, 2010, **53**, 1126.
- 18 N. Mahata, O. S. G. P. Soares, I. Rodríguez-Ramos, M. F. R. Pereira, J. J. M. Órfão and J. L. Figueiredo, *Appl. Catal., A*, 2013, **464–465**, 28.
- 19 H. Zhu, W. F. Han, H. F. Chai and H. Z. Liu, *Chin. J. Catal.*, 2007, **28**, 196.
- 20 P. R. Shukla, S. B. Wang, H. Q. Sun, H. M. Ang and M. Tadé, *Appl. Catal., B*, 2010, **100**, 529.
- 21 A. Shukla, R. K. Singha, T. Sasaki and R. Bal, *Green Chem.*, 2015, **17**, 785.
- 22 W. J. Li, L. M. Ye, P. Long, J. Chen, H. Ariga, K. Asakurab and Y. Z. Yuan, *RSC Adv.*, 2014, **4**, 29072.
- 23 J. Gong, K. Yao, J. Liu, Z. W. Jiang, X. C. Chen, X. Wen, E. Mijowska, N. N. Tian and T. Tang, *J. Mater. Chem. A*, 2013, **1**, 5247.
- 24 L. Olsson and E. Fridell, *J. Catal.*, 2002, **210**, 340.



- 25 J. L. Zhang, Y. Wang, H. Ji, Y. G. Wei, N. Z. Wu, B. J. Zuo and Q. L. Wang, *J. Catal.*, 2005, **229**, 114.
- 26 X. X. Han, R. X. Zhou, G. H. Lai and X. M. Zheng, *Catal. Today*, 2004, **93–95**, 433.
- 27 C. Lian, H. Q. Liu, C. Xiao, W. Yang, K. Zhang, Y. Liu and Y. Wang, *Chem. Commun.*, 2012, **48**, 3124.
- 28 H. M. Liu, H. B. Yu, C. R. Xiong and S. H. Zhou, *RSC Adv.*, 2015, **5**, 20238.
- 29 C. S. Lu, M. J. Wang, Z. L. Feng, Y. N. Qi, F. Feng, L. Ma, Q. F. Zhang and X. N. Li, *Catal. Sci. Technol.*, 2017, **7**, 1581.

